PHILOSOPHICAL MAGAZINE A, 1994, VOL. 70, NO. 4, 641–656

Toughness of an interface along a thin ductile layer joining elastic solids

By VIGGO TVERGAARD

Solid Mechanics Department, Technical University of Denmark, Building 404, 2800 Lyngby, Denmark

and JOHN W. HUTCHINSON

Division of Applied Sciences, Harvard University, Cambridge, Massachusetts 02138, USA

[*Received 8 March 1994 and accepted 13 April 1994*]

ABSTRACT

The contribution of plastic deformation to the effective work of fracture is computed for a crack lying along one of the interfaces of a thin ductile layer joining two elastic solids. A model is proposed for the joint whose major parameters are the layer thickness, the elastic–plastic properties of material in the layer, and the work of separation and peak separation stress of the local interface fracture process. A symmetric mode I loading of the joint is considered under conditions where the thickness of the layer and the extent of the plastic zone are small compared with the crack length. The crack growth resistance behaviour is computed, with special emphasis on the steady-state work of fracture. The role of the layer thickness in the development of the plasticity contribution to toughness is detailed. Plastic dissipation is fully realized for layers above a certain thickness, characteristic of a plastic zone dimension, and is negligible when the layer is thin relative to this dimension. Other factors which may effect the effective toughness of the joint, such as modulus mismatch of the layer and adherends and residual stress in the layer, are discussed together with limitations and possible extensions of the model.

§ 1. INTRODUCTION

It has long been appreciated that plastic dissipation contributes significantly to the total work of fracture in metals and polymeric solids. Irwin and Orowan independently argued that Griffith's energy balance for brittle crack advance must include a contribution from plastic deformation when applied to nearly all structural metals. Beyond the qualitative understanding that plastic deformation significantly adds to the toughness of ductile metals, there is little available in the way of a quantitative theory of toughness enhancement due to plasticity. In the case of cleavage fracture, for example, there is no accepted theory for predicting the consequent reduction in the plasticity contribution to the total work of fracture stemming from the reduction in the atomistic work of fracture due to an embrittling agent. Similarly, for metals which fracture by the nucleation, growth and coalescence of voids, the resultant effect on the macroscopic toughness and subsequent crack growth resistance due to alteration of conditions of void nucleation, for example, is not yet within the realm of quantitative prediction. In both instances, the missing element is the nonlinear coupling between the near-tip fracture process and the overall plastic dissipation.

Recent experiments on the toughness of joint systems consisting of a thin layer of

Fig. 1

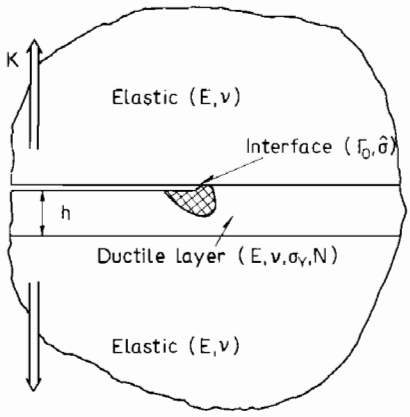

Geometry of the ductile layer problem.

ductile metal or polymeric adhesive sandwiched between two elastically deforming adherends have added new possibilities to the experimental investigation of this coupling. Reimanis *et al.* (1990) and Reimanis, Dalgleish and Evans (1991) have performed experiments on systems with a thin gold layer joining two sapphire (Al_2O_3) adherends, where a long crack is introduced on one of the gold–sapphire interfaces. The system allows direct visualization of the interface ahead of the crack tip though the transparent sapphire. Depending on the bonding process and on environmental conditions under which the test is conducted, the fracture process was observed to be either a cleavage-like interfacial separation or a void growth and coalescence mechanism occurring at the interface. The total work of fracture was found to be many times the work of the fracture process and, moreover, a fairly strong function of the thickness of the ductile gold layer. The Al_2O_3/Au sandwich system and others like it make possible systematic exploration of the role of plasticity in contributing to fracture toughness.

Plasticity also plays a significant role in the toughness of polymeric adhesive joints. Chai (1986, 1993) has carried out systematic studies of the effect of layer thickness on the macroscopic toughness of joints loaded symmetrically (mode I) and antisymmetrically (mode II). A variety of fracture process mechanisms have been observed which depend on the quality of the bond, the ductility of the adhesive material, and the type of loading. Most relevant to the present study are observations of mode I failures occurring along one of the bond interfaces and the dependence of the measured toughness of the joint on the adhesive layer thickness.

The geometry of the problem addressed in this paper is shown in fig. 1. A thin ductile layer joins two elastic blocks with identical elastic properties. A crack lies along a portion of one of the interfaces between the layer and the blocks. The crack is assumed to be sufficiently long compared with the thickness of the layer such that the effect of a remote symmetric loading is communicated to the vicinity of the crack tip through the mode I stress intensity factor K. Thus the asymptotic problem depicted in fig. 1 is a plane strain problem with two identical semi-infinite elastic blocks joined by a ductile layer of thickness h. A semi-infinite crack lies long the upper interface, and the remote plane strain field is fully specified by the applied mode I stress intensity factor K. Interface separation will be characterized by a traction-separation law, detailed shortly,

which has a work of separation per unit area denoted by Γ_0. The mechanics problem posed here is the determination of the macroscopic, or effective, work Γ of fracture per unit area in terms of Γ_0 and the properties of the layer, including its yield strength σ_Y, its strain-hardening exponent N and its thickness. A standard elastic–plastic constitutive model for metals will be used to represent the layer material. Thus the primary emphasis here will be on systems with a ductile metal layer. However, the work should also have implications for adhesive joints, to the extent that continuum metal plasticity is capable of modelling features of inelastic polymer behaviour.

Specifically, for a given set of properties, the resistance to crack advance will be determined in the form of the relation between Γ and crack advance Δa. Particular emphasis is placed on the toughness level Γ_{ss} attained after sufficient crack advance such that steady-state propagation is in effect. This paper builds on work in two earlier papers by the present authors in which the fracture process is modelled as a traction-separation law applied along the line of the crack within a continuum representation of an elastic–plastic solid. The first of these papers applied the approach to small-scale-yielding mode I crack growth in a homogeneous elastic–plastic solid (Tvergaard and Hutchinson 1992, hereafter denoted TH1). The second was concerned with mixed-mode crack growth along a bimaterial interface under small scale yielding conditions (Tvergaard and Hutchinson 1993, hereafter denoted TH2). The approach of embedding a traction-separation law within an elastic–plastic continuum to model crack growth initiation and advance was initiated by Needlehams (1987) in his study of the debonding of hard particles in ductile metal matrices.

1.1. *The traction-separation law of the interface*

Following the notation for the law introduced in TH2, let δ_n and δ_t be the normal and tangential components of the relative displacement of the crack faces across the interface in the zone where the fracture processes are occurring, as indicated in fig. 2. Let δ_n^c and δ_t^c be critical values of these displacement components and define a single non-dimensional separation measure as

$$\lambda = \left[\left(\frac{\delta_n}{\delta_n^c}\right)^2 + \left(\frac{\delta_t}{\delta_t^c}\right)^2\right]^{1/2}, \tag{1}$$

such that the tractions drop to zero when $\lambda = 1$. With $\sigma(\lambda)$ displayed in fig. 2, a potential from which the tractions are derived is defined as

$$\Phi(\delta_n, \delta_t) = \delta_n^c \int_0^\lambda \sigma(\lambda')\, d\lambda'. \tag{2}$$

Fig. 2

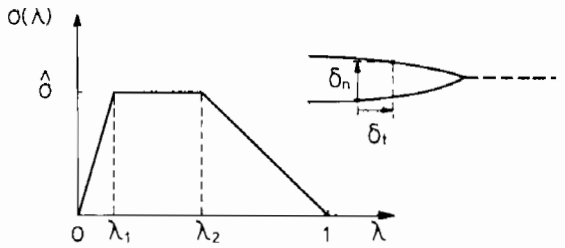

Specification of traction-separation relation.

The normal and tangential components of the traction acting on the interface in the fracture process zone are given by

$$T_n = \frac{\partial \Phi}{\partial \delta_n} = \frac{\sigma(\lambda)}{\lambda}\frac{\delta_n}{\delta_n^c}, \quad T_t = \frac{\partial \Phi}{\partial \delta_t} = \frac{\sigma(\lambda)}{\lambda}\frac{\delta_t}{\delta_t^c}\frac{\delta_n^c}{\delta_t^c}. \tag{3}$$

The traction law under a purely normal separation ($\delta_t = 0$), is $T_n = \sigma(\lambda)$ where $\lambda = \delta_n/\delta_n^c$. Under a purely tangential displacement ($\delta_n = 0$), $T_t = (\delta_n^c/\delta_t^c)\sigma(\lambda)$ where $\lambda = \delta_t/\delta_t^c$. The peak normal traction under pure normal separation is $\hat{\sigma}$, and the peak shear traction is $(\delta_n^c/\delta_t^c)\hat{\sigma}$ in a pure tangential 'separation'. The work of separation per unit area of interface is given by eqn. (2) with $\lambda = 1$. For the separation function $\sigma(\lambda)$ specified in fig. 2,

$$\Gamma_0 = \tfrac{1}{2}\hat{\sigma}\delta_n^c(1 - \lambda_1 + \lambda_2). \tag{4}$$

The parameters governing the separation law are therefore the work Γ_0 of the fracture process, the peak stress quantity $\hat{\sigma}$ and the critical displacement ratio δ_n^c/δ_t^c, together with the factors λ_1 and λ_2 governing the shape of the separation function. Note that use of the potential ensures that the work of separation is Γ_0 irrespective of the combination of normal and tangential displacements taking place in the process zone. Experience gained in the two earlier studies suggests that the details of the shape of the separation law are relatively unimportant. It will be seen that the present ductile layer problem involves separation displacements which are predominantly normal, such that the choice of the ratio δ_n^c/δ_t^c also has relatively little influence on the predictions of the macroscopic toughness. Thus the two most important parameters characterizing the fracture process in this model are Γ_0 and $\hat{\sigma}$. Further discussion of their interpretation is given below.

1.2. *Properties of the ductile layer and the two elastic solids*

As noted earlier, there are many parameters which influence the macroscopic toughness of the system shown in fig. 1. Some theoretical evidence will be cited in the final discussion section which suggests that differences between the elastic moduli of the layer and the adjoining solids may have a fairly significant effect on the macroscopic toughness of the system. The residual stress in the thin layer, acting parallel to the layer, is also likely to be important. Nevertheless, in this first study of the ductile layer system using the present approach, the effects of elastic mismatch and residual stress in the layer will not be considered. The layer and the adjoining adherends are taken to have identical isotropic elastic properties, with Young's modulus E and Poisson's ratio ν. The adherends do not yield. The layer is assumed to be stress free in the unloaded state. The layer material is characterized by J_2 flow theory, that is the standard isotropic hardening incremental plasticity theory based on the Mises invariant. The tensile curve of true stress against true strain for the layer material is taken to be

$$\varepsilon = \begin{cases} \dfrac{\sigma}{E}, \\ \dfrac{\sigma_Y}{E}\left(\dfrac{\sigma}{\sigma_Y}\right)^{1/N}, \end{cases} \quad \text{for} \quad \begin{cases} \sigma \leqslant \sigma_Y, \\ \sigma > \sigma_Y, \end{cases} \tag{5}$$

where σ_Y is the tensile yield stress and N is the strain-hardening exponent.

1.3. *Definition of the macroscopic toughness measure and the reference length quantity* R_0

Irwin's relation between the energy release rate G and the stress intensity factor K for a mode I plane-strain crack in an elastic solid is

$$G = \frac{1 - \nu^2}{E} K^2. \tag{6}$$

This relation applies to the asymptotic problem of fig. 1 with G interpreted as the remote or applied energy release rate and K as the intensity of the remote field. The crack growth resistance Γ is identified with G under conditions of crack advance. The model will be used to compute the history of Γ as a function of crack advance Δa as it depends on the parameters of the system. From these resistance curve data, one can identify a toughness level characterizing initiation of crack growth and an asymptote, denoted by Γ_{ss}, characterizing steady-state crack growth. Dimensional considerations dictate that the resistance curve will be a dimensionless function of the following non-dimensional quantities:

$$\frac{\Gamma}{\Gamma_0} = F\left[\frac{\Delta a}{R_0}, \frac{h}{R_0}, \frac{\hat{\sigma}}{\sigma_Y}, N, \frac{\sigma_Y}{E}, \nu, \frac{\delta_n^c}{\delta_t^c}, \lambda_1, \lambda_2\right], \tag{7}$$

where R_0 is a material-based reference length introduced next.

When plasticity makes a negligibly small contribution to the toughness of the system, the crack will propagate along the interface at a constant applied energy release rate equal to the work of the fracture process: $\Gamma = \Gamma_0$ or, equivalently, at $K = K_0$ where $K_0 = [E\Gamma_0/(1 - \nu^2)]^{1/2}$. As in TH1, define a reference length by

$$R_0 \equiv \frac{1}{3\pi}\left(\frac{K_0}{\sigma_Y}\right)^2 = \frac{1}{3\pi(1 - \nu^2)} \frac{E\Gamma_0}{\sigma_Y^2}. \tag{8}$$

In general, R_0 should simply be regarded as a material-based length quantity. However, under certain circumstances it can be interpreted as a plastic zone size. For a homogeneous elastic–plastic solid, R_0 is the widely used estimate of the size of the plastic zone in small-yielding under plane strain when the *remote loading* is K_0. For the present problem, R_0 can thus be regarded as an estimate of the plastic zone size, as long as it is less than the layer thickness and as long as the plasticity contribution to the macroscopic work of fracture is comparable with Γ_0. When Γ is larger than Γ_0, the plastic zone scales with but is larger than R_0.

§ 2. Identification of Γ_0 and $\hat{\sigma}$ for two fracture processes

For situations where failure of the interface predominantly involves a normal separation, it has already been remarked that the two most important parameters specifying the traction-separation law are Γ_0 and $\hat{\sigma}$. For a given application, these parameters can be regarded as phenomenological quantities and assigned values to fit the model to selected experimental resistance curve data. More fundamentally, when the essence of a given fracture process is captured by a traction-separation law such as that introduced above, there is the possibility of estimating the values of these two parameters by micromechanics analysis. An illustration of this more fundamental approach was given in TH1, where a micromechanics analysis of the mechanism of void growth and coalescence led to identification of the two parameters for this fracture process. The outcome of that analysis will be briefly reviewed, followed by a second

example for a cleavage mechanism where the representation must be regarded as phenomenological.

2.1. *Fracture process based on the mechanism of void growth and coalescence*

In TH1 the model of void growth and coalescence of Gurson (1977) was used to calculate the traction-displacement relation for a planar sheet of uniformly spaced voids sandwiched between two blocks undergoing normal separation. Under conditions discussed in TH1, where the fracture process zone extends ahead of the crack tip by more than a few void spacings, the traction-displacement relation so calculated can be used as an approximation for the separation law in the crack propagation model. In this way, one can calculate the values of Γ_0 and $\hat{\sigma}$ in terms of the parameters specifying the Gurson model. The calculations performed in TH1 give, as the work of the fracture process, $\Gamma_0 = C\sigma_Y d$, where d is the void spacing and C ranges between 0·4 and 0·8 depending on σ_Y and N. With d specified, the work of separation is otherwise only weakly dependent on the initial void volume fraction f_0. The peak stress $\hat{\sigma}$ is quite sensitive to f_0, as well as to N and σ_Y/E. A set of results taken from TH1 are reproduced in fig. 3 showing the dependence of $\Gamma_0/\sigma_Y d$ and $\hat{\sigma}/\sigma_Y$ on f_0 and N for $\sigma_Y/E = 0{\cdot}003$ and $\nu = 0{\cdot}3$.

Shih and Xia (1993) have employed a more elaborate model of the void growth and coalescence mechanism to generate plane-strain crack growth resistance behaviour. Within a finite-element representation of a solid containing a semi-finite crack, they modelled a planar array of discrete voids spaced a distance d apart on the plane ahead of the macroscopic crack tip. The Gurson model was used to represent the response of

Fig. 3

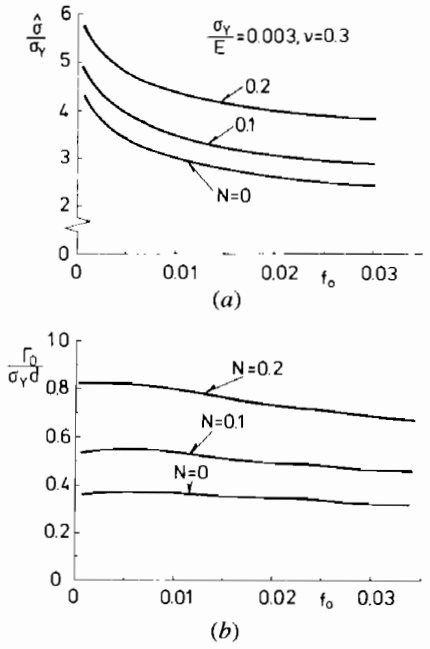

Variations in the normalized peak stress and work of fracture for the void growth and coalescence process as a function of initial void volume fraction (TH1).

the individual void cells. The predictions of the model of Shih and Xia depend on the same continuum and fracture process parameters discussed above. In the range of behaviours where the fracture process zone extends more than about two void spacings ahead of the crack tip, the predictions of their model are in close agreement with those of the present model when fracture process parameters such as those in fig. 3 are used as input.

2.2. *Fracture process based on a cleavage-like mechanism*

Suo, Shih and Varias (SSV) (1993) have proposed a model for calculating the plasticity enhancement of toughness for metals and metal–ceramic interfaces where the separation process involves atomic cleavage. They restrict consideration to metals whose structure is such that a crack tip advances by cleavage without emitting dislocations. Their emphasis is on the role of the plastic deformation which occurs as a result of generation and motion of dislocations *outside* a dislocation-free zone centred at the crack tip. Their model, which is depicted in the inset of fig. 4, uses an elastic strip of height $2D$ to represent the dislocation-free zone and uses the same isotropic hardening flow theory of plasticity referred to in § 1.2 to represent the elastic–plastic material outside the strip. Small-scale yielding in plane strain is considered with K or, equivalently, G specifying the applied field, just as in the case of the present model. Thus the SSV model is characterized by the parameters E, ν, σ_Y and N of the elastic–plastic continuum, together with the cleavage work Γ_C of fracture of the dislocation-free strip and its height $2D$. In addition to its use to predict the plasticity contribution to toughness, the SSV model was put forward to explain how stresses in the immediate vicinity of the crack tip reach the high levels needed to produce atomic

Fig. 4

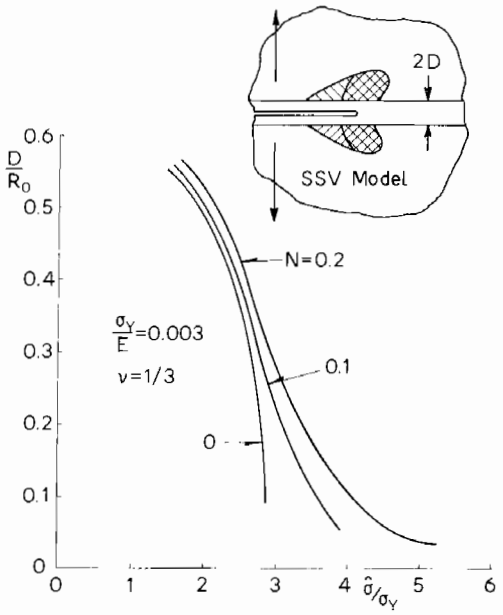

Relation of D/R_0 from the SSV model to the normalized peak stress of the present model needed to bring the steady-state toughness predictions of the two models into coincidence. Both apply to small-scale-yielding crack growth in a homogeneous elastic–plastic solid.

Fig. 5

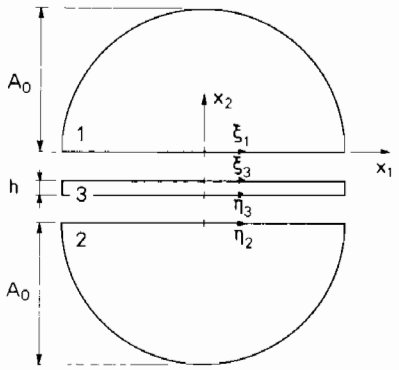

Conventions for the numerical analysis.

separation. According to standard continuum plasticity models of crack tip behaviour, stresses cannot rise to levels required for cleavage without the presence of the dislocation-free strip. The SSV model neglects a transition zone outside the dislocation-free region within which conventional continuum plasticity is obviously an inadequate representation of dislocation behaviour. Nevertheless, the model seems to capture successfully some of the main features which influence cleavage-like separation in the presence of plastic flow and appears to have qualitative validity for metals and metal–ceramic interfaces which cleave.

The present class of models does not invoke a dislocation-free elastic region and is incapable of extrapolation all the way to a crack tip undergoing cleavage-like separation. Nevertheless, it is possible to bring the present class of models into direct correspondence with the SSV class of models. Specifically, it is possible to relate Γ_0 and $\hat{\sigma}$ of the present model to Γ_C and D of the SSV model such that crack growth resistance predictions of the two models are similar. For reasons which will be made evident later in this paper, both models predict that initiation of crack growth occurs when Γ attains the local work of fracture, that is Γ_0 for the present model or Γ_C for the SSV model. Thus correspondence requires $\Gamma_0 = \Gamma_C$. The choice of $\hat{\sigma}$ is made such that the steady-state toughness Γ_{ss} predicted by the two models is also the same. Figure 4 displays plots of D/R_0 against $\hat{\sigma}/\sigma_Y$ for three values of N which achieve this purpose. (This correspondence was made using the results in fig. 5 of TH1 and the corresponding results in fig. 5 of the SSV paper, both of which were obtained with $\sigma_Y/E = 0{\cdot}003$ and $\nu = 0{\cdot}3$. The curves in fig. 4 were plotted by reading numerical values off the curves in the respective figures, and thus their accuracy may be somewhat less than the original results.) The essential point is that for D/R_0 in the range from 0·05 to 0·5 the present model can be used in a phenomenological way to reproduce the predictions of the SSV model by an appropriate choice of Γ_0 and $\hat{\sigma}/\sigma_Y$. The corresponding range of Γ_{ss}/Γ_0 is from about 20 down to 1.

In summary, in some instances, the present model can realistically reproduce behaviour down to the crack tip. In other applications, such as the SSV model of cleavage, it may be possible to choose Γ_0 and $\hat{\sigma}$ as phenomenological parameters which characterize the effective behaviour of a zone of intermediate scale surrounding the actual fracture process zone at the tip.

§ 3. Numerical method

The numerical method used to solve the present plane strain problem in fig. 1 has some similarity to the finite-element scheme used in TH1 and TH2. In particular, the numerical aspects concerned with propagation of the crack down the interface are similar to those in the interface crack study in TH2. Here, however, plastic deformation takes place only in the thin layer of thickness h, while the solids on either side of the layer remain elastic. The region analysed numerically is divided into three subregions 1, 2 and 3, as shown in fig. 5, where the outer regions 1 and 2 are semicircular with radius A_0, and region 3 is rectangular with dimensions h by $2A_0$. The finite element mesh consists of quadrilaterals, each built up of four triangular linear-displacement elements. The meshes used in regions 1 and 2 are identical with those employed in TH1 and TH2. In region 3 the quadrilaterals are rectangular with edge nodes located so that they fit the edge nodes of the adjacent region. The initial crack tip is located at $x_1 = x_2 = 0$, and a uniform mesh region of length B_0 is used in front of the initial crack tip to model crack growth. The length of one square element in this uniformly meshed region is denoted by Δ_0.

It is imagined that the extent of the plastic zone in the layer is very small compared with the full crack length. This permits consideration of the asymptotic problem depicted in fig. 1 for a semi-infinite crack under remote mode I loading. Thus, on the circular edges of regions 1 and 2, loads corresponding to the tractions of the mode I stress field are applied, with amplitude K. At the two ends of the thin layer the edge loads are neglected which introduces a very small error as long as h/A_0 is small. At the boundary between regions 2 and 3 the conditions to be satisfied are

$$u^1(\eta_3) = u^1(\eta_2), \qquad u^2(\eta_3) = u^2(\eta_2), \tag{9}$$

$$T^1(\eta_3) = -T^1(\eta_2), \quad T^2(\eta_3) = -T^2(\eta_2), \tag{10}$$

where η_2 and η_3 are coordinates along the boundary. At the boundary between regions 1 and 3 the initial crack surfaces for $x_1 < 0$ are traction free, while for $x_1 > 0$ the displacements and tractions are related by the traction-separation law of the interface of § 1.1. Thus, for $\xi_1 > 0$ and $\xi_3 > 0$ (see fig. 5)

$$u^1(\xi_1) - u^1(\xi_3) = \delta_t(\xi_3), \qquad u^2(\xi_1) - u^2(\xi_3) = \delta_n(\xi_3), \tag{11}$$

$$T^1(\xi_1) = -T^1(\xi_3) = T_t(\xi_3), \quad T^2(\xi_1) = -T^2(\xi_3) = T_n(\xi_3). \tag{12}$$

For region 1 the linear elastic equations are solved once at the start to obtain linear relations between the nodal displacements along $\xi_1 = 0$, the corresponding nodal forces, and the load amplitude K, using a Rayleigh–Ritz finite-element method (Tvergaard 1976). For region 2, similar linear relations are obtained between nodal displacements on the boundary edge with coordinate η_2, the corresponding nodal forces and the amplitude K. In the region 3, elastic–plastic deformations take place following a finite strain generalization of J_2 flow theory, as has been described in more detail in TH1. Thus for region 3 the solutions have to be obtained incrementally and, in each increment, linear relations are obtained between nodal displacement increments and the corresponding nodal forces increments on the edge $\xi_3 > 0$ and along the edge with coordinate η_3.

The linear relations for the three subregions are finally assembled using eqns. (9)–(12) to obtain a set of linear algebraic equations for the increment in the load amplitude K and the nodal displacement increments along $\xi_1 > 0$ and $\xi_3 > 0$ and along the edge with coordinate η_3. On the initial part of the resistance curve, an increment

in K is prescribed, but this procedure is unstable when K approaches its asymptote. Then, the Rayleigh–Ritz method is used to control a monotonic increase in displacement differences at the crack tip, such as those specified in eqn. (11).

In most of the computations, the properties of the elastic–plastic layer are characterized by the parameters $\sigma_Y/E = 0{\cdot}003$, $\nu = \frac{1}{3}$ and $N = 0{\cdot}1$, and the separation law is specified using $\delta_n^c/\delta_t^c = 1$, $\lambda_1 = 0{\cdot}15$ and $\lambda_2 = 0{\cdot}5$ with $\hat{\sigma}/\sigma_Y$ varied. Selected results will be reported for other values of N and δ_n^c/δ_t^c. The influence of δ_n^c/δ_t^c on the predictions in this paper will be seen to be minor.

Let Δ_0 denote the length of one of the small elements in the uniform mesh along the interface in the crack growth region. Nearly all the computations have been carried out for a region size specified by $A_0 = 9000\Delta_0$ and $B_0 = 60\Delta_0$. Computations have been carried out for various mesh refinements compared with the length scale δ_n^c of the separation law, in order to guarantee convergence of the solutions. On the basis of these trials, most of the computations have been carried out for $\delta_n^c = 0{\cdot}2\Delta_0$. For the larger values of the layer thickness h, compared with Δ_0, the mesh size is stretched across the layer in such a way that the row of quadrilateral elements along the crack plane are square. In each of the semicircular elastic regions the number of triangular elements is 7912 and the number of nodal points is 4051. In the thin elastic–plastic layer the number of triangular elements is 7808 and the number of nodal points is 4043.

§ 4. Numerical results

4.1. *Crack growth resistance curves and plastic zones*

Computed resistance curves in the form of Γ/Γ_0 as a function of normalized crack advance $\Delta a/R_0$, are shown in fig. 6 (*a*) for three values of the non-dimensional thickness h/R_0. These curves were computed with $\sigma_Y/E = 0{\cdot}003$, $\nu = \frac{1}{3}$, $N = 0{\cdot}1$ and $\hat{\sigma}/\sigma_Y = 4$. Thus the three ductile layer systems in fig. 6 have identical elastic–plastic properties and interface separation characteristics; they differ only in the thickness of the layer. Plastic zones at the point of growth where the peak value of Γ has been attained are shown in fig. 6 (*b*) for each of the three thicknesses. The non-dimensional thicknesses for the three cases have been chosen to demonstrate the strong dependence of crack growth resistance on the layer thickness. The plastic zone of the thinnest layer ($h/R_0 = 0{\cdot}37$) extends several layer thicknesses ahead of the current crack tip location. Constraint of the elastic adherends on plastic flow in the layer is known to give rise to a build-up of triaxial tension ahead of the crack (Varias, Suo and Shih 1991). Thin layers thus reach the peak stress $\hat{\sigma}$ on the interface required for crack advance at lower values of Γ, all other things being equal. The thickest layer ($h/R_0 = 5{\cdot}96$) is sufficiently thick that the plastic zone does not reach the lower adherend and is unconstrained. Since the layer and adherends have the same elastic properties, the behaviour of this system is identical with the small-scale yielding problem for a semi-infinite crack on the interface between an upper elastic half-space and a lower elastic–plastic half-space. In other words, for thicknesses in excess of a certain critical value, the thickness no longer has any influence on the effective toughness of this system. Further discussion of the transition values of thickness will be given later. The intermediate thickness ($h/R_0 = 1{\cdot}49$) gives rise to a plastic zone which is roughly the size of the layer thickness. Some interaction with the lower adherend takes place, leading to slightly lower crack growth resistance than that displayed by the thickest layer.

Initiation of crack growth is coincident with G attaining Γ_0, as can be seen in fig. 6 (a). As discussed in TH1 and TH2, this is a consequence of two theoretical features

Fig. 6

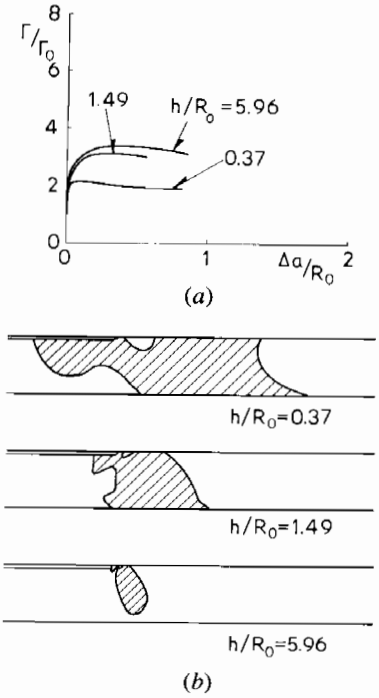

(*a*) Typical resistance curves for three values of h/R_0, corresponding to layers which can be characterized as being thin, of intermediate thickness and thick as far as plasticity effects are concerned. (*b*) Associated plastic zones at the point where the maximum Γ is attained.

associated with the model. As in most crack problems involving monotonic loading, stressing in the elastic–plastic layer is nearly proportional prior to any crack growth, and thus conditions for applicability of a deformation theory of plasticity are met. This being the case, the J integral can be used to connect the remote field with amplitude K to the separation at the end of the fracture process zone, by a procedure which is now widely known. It follows that the first attainment of separation at the end of the process zone (i.e. $\lambda = 1$ at $x_1 = 0$) requires $K = K_0$ or, equivalently, $G = \Gamma_0$.

The plastic zones in fig. 6 (*b*) are associated with the point of crack advance where the peak value of Γ is attained. The usefulness of the reference length R_0 in eqn. (8) as a measure of the plastic zone size at initiation may be evaluated by considering the plastic zone size at $\Gamma = \Gamma_0$ in the three cases in fig. 6 (*b*). For $h/R_0 = 5{\cdot}96$ the size of the plastic zone at initiation is given by the dimensions $0{\cdot}95R_0$ and $1{\cdot}69R_0$ in the directions along the layer and transverse to the layer respectively. For $h/R_0 = 1{\cdot}49$ the same dimensions are $0{\cdot}95R_0$ and h respectively and, for $h/R_0 = 0{\cdot}37$, $0{\cdot}69R_0$ and h. The first of these three cases involves no interaction between the lower adherend and the plastic zone, while in the other two the plastic zone has reached the lower adherend prior to initiation. The reference length R_0 gives a rather good estimate of the plastic zone size at $\Gamma = \Gamma_0$. Ozdil and Carlsson (1992) give further details of the relation between the plastic zone of the stationary crack to Γ computed specifically for several polymeric adhesive layers, with pressure dependence of yielding taken into account.

The slope of the resistance curve at initiation is quite high when the interface has

a high value of $\hat{\sigma}/\sigma_Y$, falling off gradually as the crack advances. The resistance curves in fig. 6 (*a*) have a shallow peak and approach their asymptotes from above. A similar behaviour was observed for some of the computed resistance curves for interface growth in TH2. In no case was the difference between the peak resistance and the asymptote appreciable. For convenience and to limit computational, effort, Γ_{ss} will be identified with the peak value of Γ rather than with the steady-state asymptote.

4.2. *Thickness dependence of steady-state toughness*

Extensive resistance curve computations have been carried out to determine the dependence of the peak crack growth resistance Γ_{ss} on the non-dimensional thickness h/R_0 and on the normalized maximum separation stress $\hat{\sigma}/\sigma_Y$ of the interface. The complete set of results for $\sigma_Y/E = 0{\cdot}003$, $\nu = \frac{1}{3}$ and $N = 0{\cdot}1$ are plotted in fig. 7. Considerable effort was made to assure the accuracy of these results. Refinements of the mesh described in § 3 and refinement of crack growth increments were carried out to establish the adequacy of the choices used in the calculations. Particularly stringent conditions exist for the larger values of $\hat{\sigma}/\sigma_Y$, and the curve for $\hat{\sigma}/\sigma_Y = 4{\cdot}5$ in fig. 7 was terminated at the value of h/R_0 shown because it was not possible to obtain accurate results for Γ_{ss} at larger values of the thickness parameter.

Several aspects of the roles of h/R_0 and $\hat{\sigma}/\sigma_Y$ are evident in fig. 7 but, nevertheless, worthy of comment. Only for $\hat{\sigma}/\sigma_Y$ larger than about 2·5 is there any significant enhancement of toughness by plasticity, as was demonstrated and discussed in the two earlier studies, TH1 and TH2. Consequently, only for $\hat{\sigma}/\sigma_Y$ larger than about 2·5 is there any significant effect of thickness on the toughness. The non-dimensional thickness needed to give the maximum possible toughness enhancement, $(\Gamma_{ss})_{max}/\Gamma_0$, depends on $\hat{\sigma}/\sigma_Y$. For the highest levels of enhancement shown in fig. 7 (i.e. $\Gamma_{ss}/\Gamma_0 = 6$ for $\hat{\sigma}/\sigma_Y = 4{\cdot}25$) a value of h/R_0 larger than about 4 is needed. Recall that, for thicknesses above this transition level, negligible interaction occurs between the plastic zone and the lower adherend for a system with homogeneous elastic properties. Included in fig. 7 as a broken curve is the approximate location of the transition, h_c/R_0. Layer thicknesses in excess of h_c ensure that the full plasticity enhancement of toughness occurs, while smaller thicknesses experience constraint from the lower adherend which reduces

Fig. 7

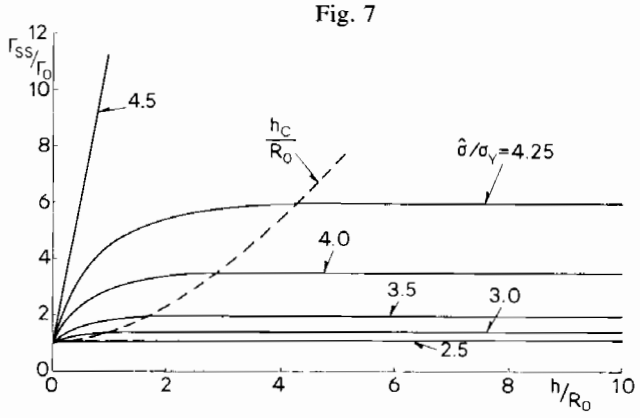

The dependence of Γ_{ss}/Γ_0 on normalized layer thickness h/R_0 ($N = 0{\cdot}1$; $\sigma_Y/E = 0{\cdot}003$; $\nu = \frac{1}{3}$): (– – –) the minimum value of the normalized thickness h_c/R_0 needed to realize the maximum possible contribution of plasticity to toughness.

the plasticity contribution. The larger the maximum possible plasticity contribution to the toughness relative to Γ_0, the larger must be the layer thickness relative to R_0 to attain it.

Figure 7 suggests an experimental procedure to obtain the 'intrinsic' or local work Γ_0 of fracture. In principle, by measuring the steady-state toughness Γ_{ss} for a sequence of specimens with decreasing layer thickness, one could extrapolate to thickness levels such that $\Gamma_{ss} = \Gamma_0$. Figure 7 gives an indication of the range of thicknesses required to carry out this extrapolation. If, for example, the process of testing a sequence of specimens suggests that the toughness of the systems with the thickest layers ($h > h_c$) is $6\Gamma_0$, then the normalized layer thicknesses h/R_0 in the sequence should range from less than about $\frac{1}{4}$ to about 4. Since Γ_0 is involved in the definition of both R_0 and h_c, the process in inherently implicit.

The strain-hardening exponent N is the most important of the non-dimensional continuum parameters of the elastic–plastic layer listed in eqn. (7) influencing crack growth resistance. Figure 8 displays the maximum possible plasticity enhancement $(\Gamma_{ss})_{max}/\Gamma_0$ as a function of $\hat{\sigma}/\sigma_Y$ for two values of N. The values for $N = 0{\cdot}2$ were computed using $h/R_0 > 6$ and thus satisfied the condition $h > h_c$ for all values of $\hat{\sigma}/\sigma_Y$ shown. The values of $(\Gamma_{ss})_{max}/\Gamma_0$ for $N = 0{\cdot}1$ are the asymptotes for large h/R_0 in fig. 7. Higher levels of strain hardening permit larger stresses to develop at the crack tip and, for a given value of $\hat{\sigma}/\sigma_Y$, lead to lower toughnesses. The trend with N in fig. 8 is similar to that observed for crack growth in homogeneous solids in TH1. The effect of σ_Y/E on the non-dimensional crack growth relation (7) was also explored in that earlier study and was found to be minor. It is expected to have a secondary role in the present problem as well.

Fig. 8

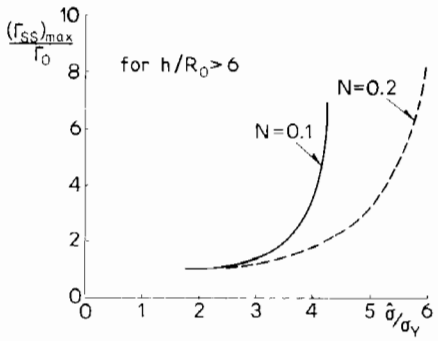

Toughness $(\Gamma_{ss})_{max}/\Gamma_0$ of joints with thick layers against $\hat{\sigma}/\sigma_Y$ for two N values.

Values of $(K_{ss})_{max}/K_0$ for various δ_n^c/δ_t^c.

	$(K_{ss})_{max}/K_0$		
δ_n^c/δ_t^c	$h/R_0 = 0{\cdot}37$	$h/R_0 = 1{\cdot}49$	$h/R_0 = 5{\cdot}96$
1	1·46	1·77	1·85
2	1·46	1·77	1·85
0·5	1·49	1·79	1·86
10	1·46	1·78	

The effect of δ_n^c/δ_t^c has been checked by a number of computations for the three cases illustrated in fig. 6. Owing to the different behaviours of the materials on either side of the interface containing the crack, the stress fields at the crack tip are not symmetric and shear, as well as normal, tractions occur on the interface. Thus the tangential component of the relative crack face displacement δ_t is expected to play some role in the separation process, although it proves to be minor. Changing δ_n^c/δ_t^c from the value of unity used in nearly all the calculations resulted in almost no change in the predicted resistance curves. The table displays the values of $(K_{ss})_{max}/K_0$ computed for three other choices of δ_n^c/δ_t^c for three values of normalized thickness.

§ 5. Discussion

The problem of linking up an atomic separation process through various scales, through a plastic zone to an outer field, is clearly a major challenge which the present model does not pretend to address. At a less fundamental level, the model does permit conclusions to be drawn about the contribution of plastic deformation in the ductile layer to the effective work of fracture of the interface. The enhancement due to plasticity, reflected in the ratio Γ_{ss}/Γ_0, depends on the properties of the layer (primarily on its strain-hardening exponent N), on the traction-separation law employed to model the fracture process (primarily on $\hat{\sigma}/\sigma_Y$) and on the non-dimensional thickness h/R_0 of the layer. As discussed in § 2, the traction-separation law may in some applications model details of an actual fracture process mechanism (but *not* an atomic separation process), while in others it may be used as a phenomenological characterization of a fracture mechanism occurring on a finer scale. Plasticity enhancements of toughness in the range from zero up to about ten times the 'intrinsic' work Γ_0 of the fracture process have been computed. This is the range in which the model is primarily applicable. Higher levels of Γ_{ss}/Γ_0 would be associated with even higher values of the normalized peak traction $\hat{\sigma}/\sigma_Y$ of the fracture process than those shown, for example, in fig. 8. The continuum plasticity model used to represent the layer material (J_2 flow theory) does not give rise

Fig. 9

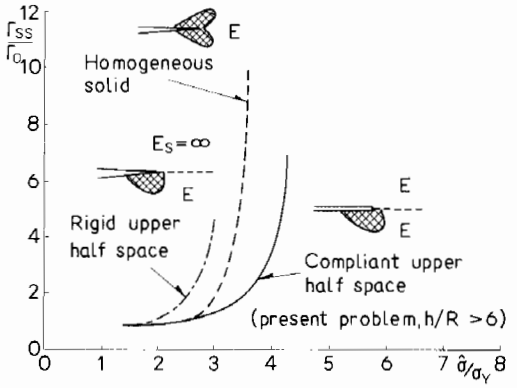

Comparison of steady-state small-scale-yielding mode I toughnesses as predicted by the present model for three systems. In decreasing order of toughness: a bimaterial interface joining an elastic–plastic solid with a rigid solid; a homogeneous elastic–plastic solid; a bimaterial interface joining an elastic–plastic solid with an elastic solid where both solids have identical elastic moduli. The traction-separation law is the same for all three cases, and in each case $N = 0{\cdot}1$ and $\sigma_Y/E = 0{\cdot}003$ ($\nu = \frac{1}{3}$ for the interface problems and $\nu = 0{\cdot}3$ for the homogeneous system).

to normalized stresses in the vicinity of the crack tip much higher than the highest levels of $\hat{\sigma}/\sigma_Y$ terminating the curves in fig. 8. Thus prediction of larger values of Γ_{ss}/Γ_0 than those determined here would require either the modification of the representation of the fracture process or the use of a plasticity theory more realistically capable of capturing the higher stresses generated under the high strain gradients present at the crack tip.

Figure 9 provides a comparison between steady-state mode I crack growth resistance results computed with the present model for three different applications. The curve for the present layer problem is taken from fig. 8, corresponding to the asymptotic limiting toughness for large layer thicknesses. As has already been emphasized, this curve applies equally well to the small-scale-yielding problem for a crack on an interface between two semi-infinite blocks with identical elastic properties, with plastic yielding occurring only in the lower block. The curve for Γ_{ss}/Γ_0 in mode I growth in small scale yielding in a homogeneous solid was taken from TH1, while the curve for small-scale-yielding growth along a bimaterial interface where the half-space block above the interface is rigid was taken from TH2. For each value of $\hat{\sigma}/\sigma_Y$, the value of Γ_{ss}/Γ_0 on this latter curve was chosen as the *minimum* value over the entire range of mixed-mode loadings and thus can be regarded as the 'mode I' steady-state toughness of the bimaterial interface.

The three sets of results in fig. 9 were computed with identical parameters governing the elastic–plastic behaviour ($N = 0{\cdot}1$; $\sigma_Y/E = 0{\cdot}003$; $\nu = \frac{1}{3}$) and the traction-separation law for the interface ($\lambda_1 = 0{\cdot}15$; $\lambda_2 = 0{\cdot}5$; $\delta_n^c/\delta_t^c = 1$). (The results of TH1 were for $\nu = 0{\cdot}3$ and not $\frac{1}{3}$, but that difference should have negligible effect.) The significant differences in predicted toughness for the three systems are due to 'extrinsic' factors. Consider first the difference between the toughness for mode I growth in the homogeneous material and that for interface growth where the elastic properties are homogeneous but yielding occurs only below the interface. At the simplest level of reasoning, it is expected that the homogeneous solid should have the higher toughness of the two systems since it has two lobes making up its plastic zone, one above and one below the crack line, as opposed to just one lobe below the interface for the other system. Were the lobes of similar size for a given value of $\hat{\sigma}/\sigma_Y$, one would expect roughly twice as much plastic dissipation in the homogeneous system as in the other system. Of course, the interaction between plastic deformation and near-tip traction separation behaviour is highly nonlinear, and thus the plastic lobes for the two systems will not necessarily be of identical size, nor will the distributions of plastic strains within the lobes be the same. Nevertheless, the relative toughness of these two systems is in qualitative accord with a simple argument based on the number of lobes to the plastic zone.

Clearly, this argument does not carry over to the system which has a rigid solid above the interface ($E = \infty$ and $\sigma_Y = \infty$ for the upper solid). At a given $\hat{\sigma}/\sigma_Y$, this system has considerably higher steady-state toughness than either of the other two systems, even though it also only has plastic deformation occurring below the interface. The explanation for this apparent anomaly appears to be substantial shielding of the crack tip by the solid above the interface due to its rigidity. For an interface with a given $\hat{\sigma}/\sigma_Y$, higher levels of G are needed to propagate the crack. Plasticity is inherently involved in this effect because the discrepancy between the three systems disappears when there is no plastic contribution to the toughness. Further evidence for a significant influence of the modulus mismatch on the effective interface toughness has been obtained in computations currently under way.

In conclusion, there are many factors which can significantly influence the effective toughness of a joint consisting of a ductile layer sandwiched between two elastic solids.

In addition to 'intrinsic' properties of the interface itself (modelled here by Γ_0 and $\hat{\sigma}$), there are the properties of the elastic–plastic material in the layer, the layer thickness and, in all likelihood, the elastic mismatch between the layer and the adherends. It remains to investigate the role of residual stress in the layer. The utility of the present model is that it permits the role of these 'extrinsic' properties to be explored.

Acknowledgments

The work of J.W.H. was supported in part by the National Science Foundation (Grant No. MSS-92-02141) and by the Division of Applied Sciences, Harvard University.

References

Chai, H., 1986, *Engng Fract. Mech.*, **24,** 413; 1993, *Int. J. Fract.*, **60,** 311.
Gurson, A. L., 1977, *J. Engng Mater. Technol.*, **99,** 2.
Needleman, A., 1987, *J. appl. Mech.*, **54,** 525.
Ozdil, F., and Carlsson, L. A., 1992, *Engng Fract. Mech.*, **41,** 645.
Reimanis, I. E., Dalgleish, B. J., Brahy, M., Rühle, M., and Evans, A. G., 1990, *Acta metall. mater.*, **38,** 2645.
Reimanis, I. E., Dalgleish, B. J., and Evans, A. G, 1991, *Acta metall. mater.*, **39,** 3133.
Shih, C. F., and Xia, L., 1993, *Constraint Effects in Fracture: Theory and Applications*, ASTM Special. Publication No. 1244, edited by M. Kirk and A. Bakker (Philadelphia, Pennsylvania: American Society for Testing and Materials).
Suo, Z., Shih, C. F., and Varias, A. G., 1993, *Acta metall. mater.*, **41,** 1551.
Tvergaard, V., 1976, *J. Mech. Phys. Solids*, **24,** 291.
Tvergaard, V., and Hutchinson, J. W., 1992, *J. Mech. Phys. Solids*, **40,** 1377; 1993, *Ibid.*, **41,** 1119.
Varias, A. G., Suo, Z., and Shih, C. F., 1991, *J. Mech. Phys. Solids*, **39,** 963.